Towards improved 3D carotid artery imaging with Adaptive CaRdiac cOne BEAm computed Tomography (ACROBEAT)

Tess Reynolds[1*], Owen Dillon[1], Joseph Prinable[1], Brendan Whelan[1, 2], Paul J. Keall[1] and Ricky T. O'Brien[1]

[1]ACRF Image X Institute, Faculty of Medicine and Health, The University of Sydney, NSW 2006, Australia.

[2]Innovation, Advanced Therapies, Siemens Healthcare GmbH, Forchheim 91301, Germany

*corresponding author contact: tess.reynolds@sydney.edu.au

Abstract

Purpose: Interventional treatments of aneurysms in the carotid artery are increasingly being supplemented with 3D x-ray imaging. The 3D imaging provides additional information on device sizing and stent malapposition during the procedure. Standard 3D x-ray image acquisition is a one-size fits all model, exposing patients to additional radiation and results in images that may have cardiac-induced motion blur around the artery. Here, we investigate the potential of a novel dynamic imaging technique Adaptive CaRdiac cOne BEAm computed Tomography (ACROBEAT) to personalize image acquisition by adapting the gantry velocity and projection rate in real-time to changes in the patient's electrocardiogram (ECG) trace.

Methods: We compared the total number of projections acquired, estimated carotid artery widths and image quality between ACROBEAT and conventional (single rotation fixed gantry velocity and acquisition rate, no ECG-gating) scans in a simulation study and a proof-of-concept physical phantom experimental study. The simulation study dataset consisted of an XCAT digital software phantom programmed with five patient-measured ECG traces and artery motion curves. The ECG traces had average heart rates of 56, 64, 76, 86 and 100 bpm. To validate the concept experimentally, we designed and manufactured the physical phantom from an 8mm diameter silicon rubber tubing cast into Phytagel. An artery motion curve and the ECG trace with an average heart rate of 56 bpm was passed through the phantom. To implement ACROBEAT on the Siemens ARTIS pheno angiography system for the proof-of-concept experimental study, the Siemens Test Automation Control System was used. The total number of projections acquired and estimated carotid artery widths were compared between the ACROBEAT and conventional scans. As the ground truth was available for the simulation studies, the image quality metrics of Root Mean Square Error (RMSE) and Structural Similarity Index (SSIM) were also utilized to assess image quality.

Results: In the simulation study, on average, ACROBEAT reduced the number of projections acquired by 63%, reduced carotid width estimation error by 65%, reduced RMSE by 11% and improved SSIM by 27% compared to conventional scans. In the proof-of-concept experimental study, ACROBEAT enabled a 60% reduction in the number of projections acquired and reduced carotid width estimation error by 69% compared to a conventional scan.

Conclusion: A simulation and proof-of-concept experimental study was completed applying a novel dynamic imaging protocol, ACROBEAT, to imaging the carotid artery. The ACROBEAT results showed significantly improved image quality with fewer projections, offering potential applications to intracranial interventional procedures negatively affected by cardiac motion.

Keywords: cardiovascular, adaptive, CBCT, imaging, intervention

I. Introduction

It is estimated that 10-12 million people in the United States have an intracranial aneurysm [1]. Fortunately, the majority of these aneurysms are small, resulting in 50-80% of all aneurysms remaining intact for the duration of a person's life [2]. However for those that rupture, subarachnoid haemorrhage occurs [3, 4], resulting in high mortality rates (45% at 30 days) and a noticeable increase in disability rates among the surviving patients (~30%) [5]. Common treatment techniques for intracranial aneurysms include microsurgical clipping [6], endovascular coiling [7] and flow diversion [8]. All three techniques rely heavily on intraprocedural imaging to guide the procedure. Most commonly, 2D digital subtraction angiography (DSA) is used to characterize the aneurysm and surrounding arteries and blood vessels before, during and after the procedure. However, the information provided by 2D DSA images is not always sufficient to assess stent position or adaption of the stent struts to the vessel wall (also known as malapposition), which can lead to stroke related complications [9]. To supplement the existing imaging protocols, in-room intraprocedural 3D cone beam computed tomography (CBCT) imaging is being utilized to aid in deciding the course of treatment once the procedure has begun [10]. Examples of the added benefit of intraprocedural 3D imaging include enabling the identification of previously unseen malapposition of embolization devices during flow diversion procedures [11] and providing adequate visualisation of stent struts during stent-assisted coil embolization [12].

Single sweep, non-ECG gated DynaCT (Siemens Healthcare GmbH, Erlangen Germany) acquisitions are some of the 3D imaging protocols used during endovascular coiling and flow diversion procedures [10-14]. For these procedures, the 3D image scan occurs in a single sweep of the gantry with constant gantry rotation velocity and projection acquisition rate. The scan acquires evenly spaced projections over a 200° scan range, irrespective of the patient's cardiac cycle. On modern imaging systems, DynaCT scans can be completed quickly, with a scan time as short as 4 seconds. However, using computer simulations of blood-flow and vessel mechanics, it has been shown that for an artery with diastolic diameter of 6.2 mm, the artery will expand up to 16% over the course of the cardiac cycle, leading to a maximum diameter of 7.2 mm or 1 mm perturbation [15, 16]. Therefore, by not taking into consideration the patient's cardiac rate and imaging indiscriminately throughout the cardiac cycle, the reconstructed image may have reduced quality due to the presence of cardiac-induced motion blur around the artery. An example of imaging the carotid artery using a conventional acquisition is provided in Figure 1. Limiting cardiac-induced motion blur during image acquisition may further improve device/artery visualization, providing more information to aid in decision making during procedures.

Typically, x-ray imaging is a trade-off between radiation delivered to the patient and image quality. Previously, we have developed a dynamic imaging protocol known as Adaptive CaRdiac cOne BEAm computed Tomography (ACROBEAT) that adapts the imaging hardware (gantry velocity and projection rate with changes in a patient's electrocardiogram (ECG) signal), only acquiring individual x-ray projections within a defined acquisition window of the cardiac cycle as required, shown in Figure 1. In simulation studies ACROBEAT has demonstrated its potential to significantly reduce the total number of projections and simultaneously improve image quality by reducing cardiac motion blur [17, 18].

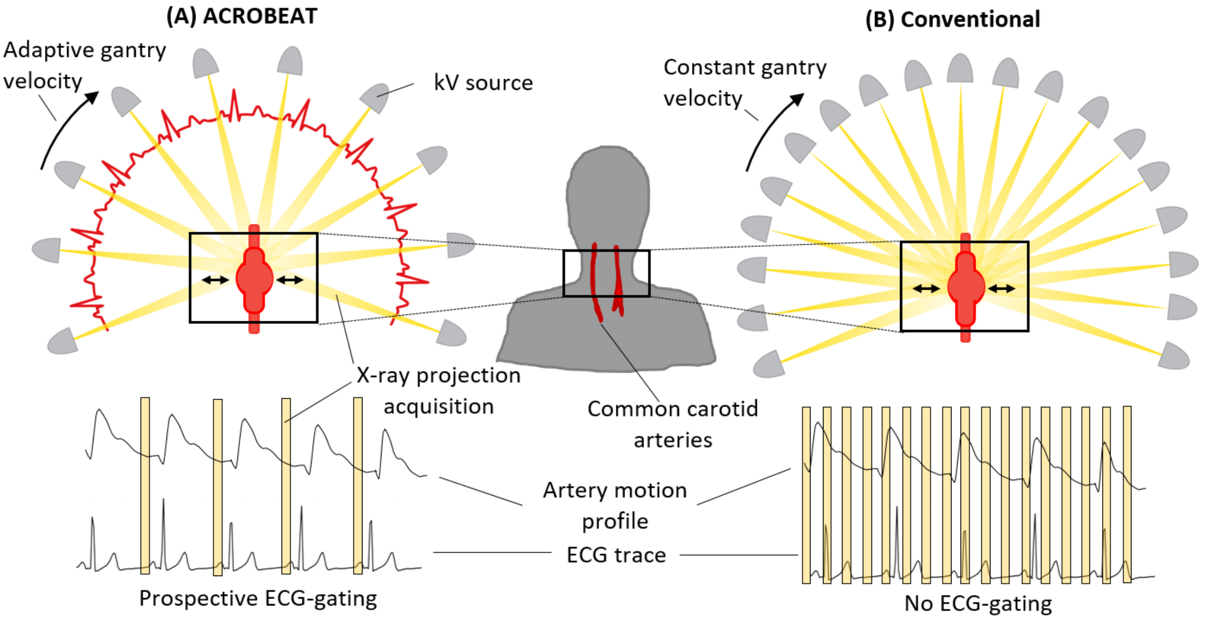

Figure 1. Carotid artery imaging via (A) ACROBEAT and (B) conventional acquisition.

Here, we use ACROBEAT to adapt the image acquisition to the patient's real-time ECG signal to reduce motion blur in carotid artery imaging. We will estimate the reduction in the total number of projections acquired and improvement in the carotid artery width measurements and image quality compared to currently utilized clinical practices for carotid artery imaging.

II. Materials and Methods

We compared the total number of projections acquired, estimated carotid artery widths and image quality between ACROBEAT and conventional (single rotation fixed gantry velocity and acquisition rate, no ECG-gating) scans in a simulation study and a proof-of-concept physical phantom experimental study.

A. Acquisition Protocols

A.1 Adaptive CaRdiac cOne BEAm computed Tomography (ACROBEAT)

ACROBEAT is a dynamic imaging protocol that adapts the gantry velocity and projection acquisition rate of the imaging hardware with respect to changes in a patient's physiological signals. Previously, ACROBEAT has been used to simulate the real-time dynamic adaption of the image acquisition of clinical CBCT imaging systems using either a patient's cardiac signal [17] or the patient's cardiac and respiratory signals [18]. The details of the decision algorithm controlling ACROBEAT are detailed elsewhere [17]. In the present work, ACROBEAT uses the patient's cardiac signal on a robotic C-arm CBCT system.

The primary aims of utilizing ACROBEAT for 3D imaging of the carotid artery are to reduce the total number of projections and maintain or improve image quality compared to the currently available in-room 3D imaging protocols. It is proposed that the total number of projections can be reduced by ensuring projections are only acquired within the desired acquisition window and that image quality can be improved by ensuring all projections are acquired with even angular spacing, Figure 2. Previous simulation studies have investigated the influence of the total number of projections acquired on total scan time and image quality for a variety of heart rates. These studies have shown that improvements in the image quality are observable via an increase in image sharpness (through the metric Edge Response Width) with as few as 40 projections (angular spacing of 5°) [18]. Further, image sharpness was also shown to not significantly improve when more than 100 projections (angular spacing of 2°) [17] were acquired. Therefore, for the simulation study and experimental test case, we aim to acquire 100 evenly spaced projections within the desired acquisition window.

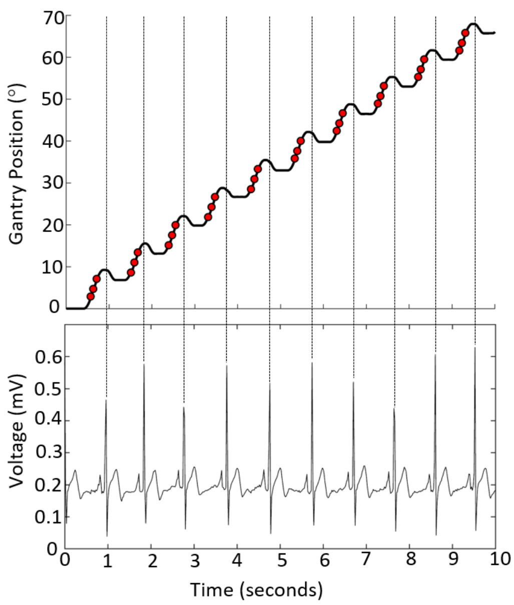

Figure 2. Dynamic imaging with ACROBEAT. The gantry trajectory (black) and timing of the projection acquisition (red circles) is adapted to the patient's ECG signal (bottom panel) as it evolves in real-time.

As we are only concerned with generating 3D images, a single acquisition window within each cardiac cycle is considered. The precise location of the acquisition window within the cardiac cycle is dependent on the desired application, with previous studies identifying the ideal time through the R-R cycle where motion of specific heart structures is minimized for various average heart rates [19-21]. Here, we select the 60-80% window for the ACROBEAT scans [17, 18].

In its current implementation, ACROBEAT uses previous cardiac cycles in a 5 second rolling window to predict future cycles. The 5 second rolling window has proven sufficient for a range of heart rates in our previous simulation studies [17, 18], including considering the effect of arrhythmic heart rates on the algorithm's performance. Note however, if the heart rate remains irregular for a long period of time, the scan would be aborted. To optimize the threshold for irregularity leading to an aborted scan would require a study to be completed with human volunteers.

In an idealized case where a patient's heart rate is constant, the ACROBEAT algorithm can ensure that all projections are acquired and that they have the required angular separation. However, this cannot be ensured with real patient ECG traces due to the ever-changing nature of a patient's heart rate and a strict condition that ensures all projections acquired reside within the designated acquisition window. The strict acquisition condition is implemented to help ensure the highest possible image quality, but the condition also leads to an increase in scan time. Instead of acquiring discriminately throughout the entire cardiac cycle, by only acquiring within the specified acquisition window, ACROBEAT needs to see more cardiac cycles to ensure complete angular coverage over the scan range, leading to an increase in scan time. Overall, the total scan time of an ACROBEAT scan is dependent on multiple factors including the patient's heart rate, scan parameters (e.g. length of the acquisition window and angular separation between projections) and mechanical constraints of the system.

A.2 Conventional

Comparatively, the conventional scan considered is based on the clinically available *syngo* DynaCT protocol (Siemens Healthcare GmbH, Erlangen, Germany). A *syngo* DynaCT, referred to throughout as the conventional scan, has constant gantry velocity and projection acquisition rate. It acquires 248 evenly spaced projections over a 200° scan range in 4 seconds, acquiring irrespective of the cardiac signal.

B. Simulation Study using a Digital Phantom (XCAT)

The Siemens ARTIS pheno (Siemens Healthcare GmbH, Erlangen, Germany) is a robotic CBCT imaging system for interventional imaging. The simulated ACROBEAT and conventional scans are performed within the listed mechanical constraints and acquisition parameters of this system. Of specific interest for ACROBEAT is the gantry rotation properties. Namely, that the gantry can accelerate and decelerate up to $200^{\circ}/s^{-2}$ and rotate at 90°/s, enabling ACROBEAT to complete its unique gantry movements, Figure 2. The maximum velocity reached by the gantry during an ACROBEAT scan is dependent on the patient's heart rate to ensure that all the required movements of the gantry can be completed within the timeframe of a single cardiac cycle.

XCAT is a digital software phantom that simulates realistic anthropomorphic anatomy and physiology [22]. The XCAT has inbuilt motion models that allow replication of breathing and cardiac motion on organs and anatomy in the thorax region. However, there are no inbuilt motion models available for anatomy in other regions of the body. As such, expansion and contraction of the carotid artery had to be completed manually. An example of the anatomically labelled volume X_{label} that was generated in XCAT alongside a volume with accurate absorption coefficients X_{static}, representing the carotid artery as it appears in the XCAT with no cardiac induced motion is shown in Figure 3 (A). All volumes, including the reconstructions, consist of 256 × 200 × 256 voxels of size 1 × 1 × 1 mm^3. Absorption coefficient in the carotid artery was $a_{contrast}$ to simulate the injection of iodine contrast agent during the scan. The carotid arteries were extracted from X_{label} to form a mask volume M_{static} where $M_{static} = 1$ at voxels containing the carotid and $M_{static} = 0$ elsewhere. In order to simulate the radial expansion of the carotid artery throughout the cardiac cycle, a spherical kernel k_r was formed with radius $r = 0.5$ mm and convolved with M_{static} to form $M_{expand} = M_{static} * k_r$. A radius of 0.5 mm was found to be the maximum radial displacement of the carotid in previous studies [23, 24]. Note that $0 < M_{expand} < 1$ in voxels only partially containing the wider carotid. A new volume with wider carotid was formed, labelled as X_{expand} that has carotid arteries with at most 1 additional voxel with absorption $a_{contrast}$ on the boundary of the carotid in X_{static}, Figure 3 (B).

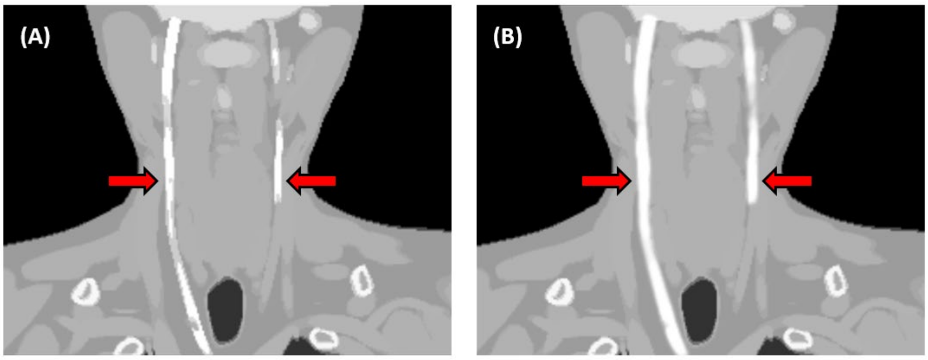

Figure 3. Coronal view of the XCAT digital phantom showing the common carotid arteries with iodine contrast (red arrows) (A) with no radial expansion (X_{static}) and (B) with the maximum 1 mm of diameter expansion (X_{expand}).

A new XCAT volume was generated for every projection required in the simulation study. The width of the carotid arteries in each volume was calculated by applying a scaling factor to the mask volume M_{expand}, $\alpha_j \sim \mathcal{N}(\mu_j, \sigma_j^2)$ that was drawn from a normal distribution where μ_j and σ_j^2 corresponding to cardiac phase ϕ_j were taken from single wall displacement data presented by Au et al. [23, 24], as shown in Figure 4. We set $\alpha_j = 0$ or $\alpha_j = 1$ when $\alpha_j < 0$ or $\alpha_j > 1$ respectively to ensure minimal and maximal radial displacements found in Au et al. [23, 24] were not exceeded. The ground truth volume generated from the XCAT phantom, $X_{GT,j}$, from which p_j was calculated as $X_{GT,j} = (1 - \alpha_j)X_{static} + \alpha_j X_{expand}$ which represents the summation of the XCAT phantom, X_{static}, with the expanded carotid, X_{expand}. Note that for the ACROBEAT acquisitions we are trying to reconstruct the carotid during the 60-80% cardiac phase window so $X_{GT,j} = 0.86X_{static} + 0.14X_{expand}$ from Au et al. [23, 24] .

Five ECG traces were sourced from the "Combined measurement of ECG, Breathing and Seismocardiogram" (CEBS) database [25, 26]. The traces were selected to represent the closest heart rate to the center of the ranges spanning 50-60 bpm, 60-70 bpm, 70-80 bpm, 80-90 bpm and 90-100 bpm. The CEBS database contains conventional ECG signals and respiratory signals obtained from a thoracic piezoresistive band and seismocardiograms from 20 healthy volunteers laying in supine position, awake, on a single bed. The ECG traces had average heart rates of 56, 64, 76, 86 and 100 bpm, corresponding to traces M007, M004, M017, M016 and M008 respectively. For simplicity, these traces will be referred to as the $\overline{56}$,$\overline{64}$, $\overline{76}$, $\overline{86}$ and $\overline{100}$ bpm traces respectively. These traces were passed through the ACROBEAT and conventional acquisition protocols (detailed in section 2.A) with the angles θ and cardiac phase φ calculated for each projection p_j. Projections for each protocol and ECG trace were simulated at a tube voltage of 90 kV as $p_j \sim \mathcal{P}\left(I_0\, e^{(-A_j X_{(GT,j)})}\right)$ where the noise is simulated by a Poisson process, $\mathcal{P}$, with a simulated photon count of $I_0 = 30{,}000$ and A_j is the forward projection matrix at angle θ_j implemented in the Reconstruction Tool Kit (RTK) [27]. The addition of noise in each projection is to ensure a realistic simulation of a CBCT acquisition. While the noise will contribute to the blurring of the artery edge (used to calculate the width of the carotid artery), the cardiac induced motion remains the dominating factor in the blurring of the artery edges. We simulated projections with Source-Isocenter Distance (SID) of 785 mm and Source-Detector Distance (SDD) of 1300 mm to a 624 × 464 pixel detector with pixel width 0.64 mm. This is the same data simulation scheme used in earlier CBCT simulation studies [40,41] adjusted for the ARTIS pheno c-arm geometry.

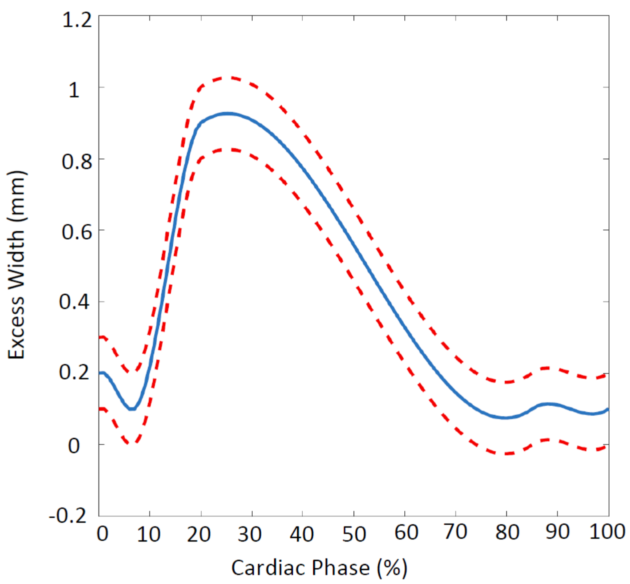

Figure 4. Expanded carotid artery width versus cardiac phase. Mean width as solid blue line, standard deviation confidence interval as dashed line. This is a reproduction of the results derived in Au et al. [23, 24].

C. <u>Proof-of-concept Physical Phantom Study on the ARTIS pheno</u>

To demonstrate the feasibility of conducting ACROBEAT scans on a clinical imaging system for carotid artery imaging, a proof-of-concept physical phantom experiment study was completed. In order to implement ACROBEAT on a clinical imaging system, a research agreement with Siemens Healthcare GmbH, Erlangen, Germany was established to provide real-time access to the control system of the robot (detailed in section C.1). A simplistic physical artery phantom was designed and manufactured to facilitate the proof-of-concept scans (detailed in section C.2).

C.1 Unique Robotic Cone Beam Imaging System

To enable real-time control of the Siemens ARTIS pheno, the Siemens Test Automation Control System (TACS) was used, Figure 5. The TACS enables control of the Control Module of the Siemens ARTIS pheno via software commands. The Control Module is comprised of individual modules responsible for controlling the movements of all the individual components of the system. Of specific interest to this work is the Pilot Control Module, which is responsible for controlling the movements of the stand and C-arm. Commands to update the stand and C-arm position with the TACS were sent via a C# DLL, Figure 5. These software commands effectively replicate the joystick control available on the physical Pilot Control Module attached to the ARTIS pheno in the examination room and in the control room. Additionally, the real-time position of the gantry is provided by a Siemens issued Research Interface computer, Figure 5. It should be noted that installation of the TACS voids the CE label of the ARTIS pheno with our ARTIS pheno dedicated to research only.

For safety reasons, the maximum gantry rotation velocity using the TACS is 20°/s; this is substantially slower than the rotation speed of normal 3D acquisitions, which is 90°/s. Due to this limited rotation speed, the ACROBEAT scans are not able to acquire multiple projections within the desired acquisition window each cardiac cycle as proposed previously [17] and in the current simulation study, Figure 2. Instead, a single projection per cardiac cycle is acquired, with the gantry rotating clockwise at a slow but variable speed. This significantly increases the total scan time of the ACROBEAT scans in the current implementation but still provides sufficient proof-of-concept.

To align with the simulation study, we aim to acquire 100 evenly spaced projections within the desired acquisition window over the 200° scan range. The total time of the scan is dependent on the patient's heart rate, with higher heart rates corresponding to shorter scan times. As we could only acquire one projection per cardiac cycle, the scan time was the length of 100 cardiac cycles.

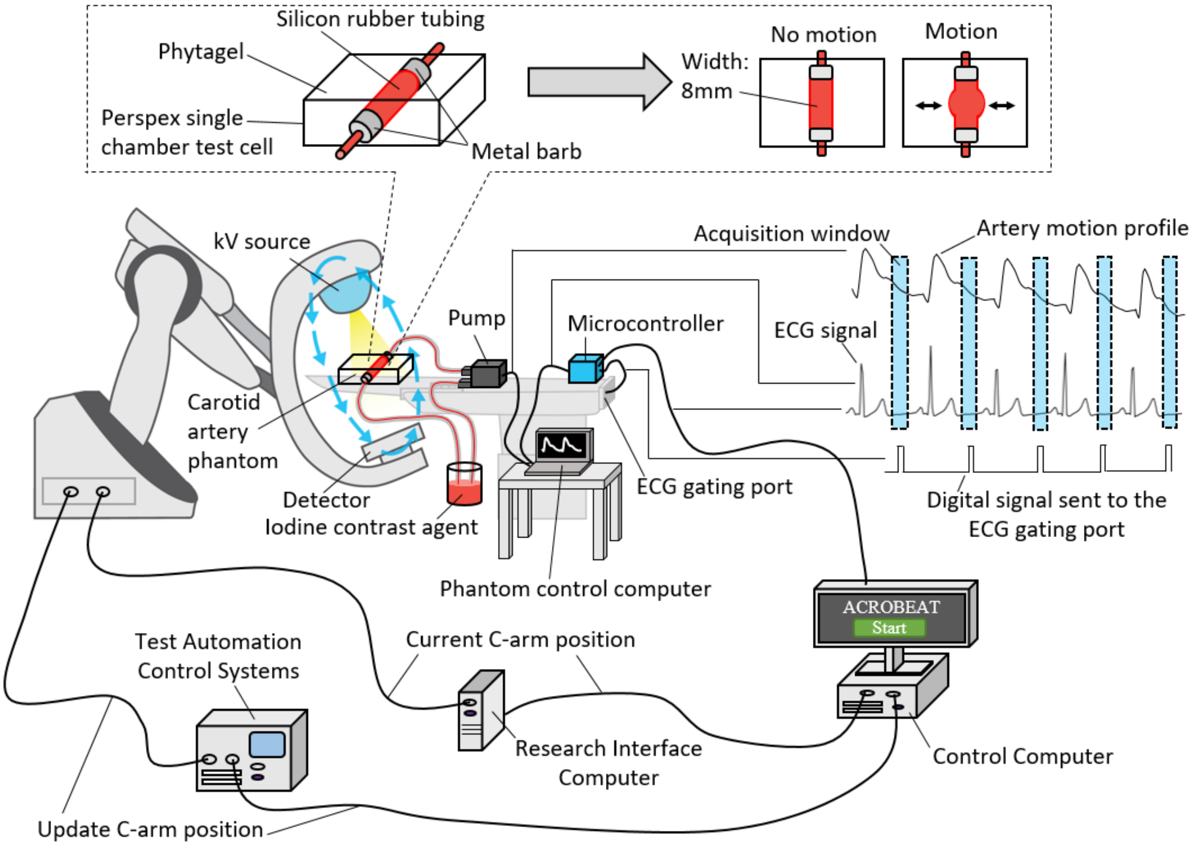

Figure 5. Experimental set up for undertaking carotid artery imaging with ACROBEAT.

The ACROBEAT system also modulates projection acquisition. In order to acquire projections when required, we used the ECG-gating port of the ARTIS pheno. The ECG gating port of the ARTIS pheno allows digital signals representing the detection of the QRS-complex of an ECG trace to be directly passed to it. For the ACROBEAT scans we selected the CORO acquisition protocol (90 kV, 24 mAs) with 'ECG-gated' as the acquisition frame rate. In general, selection of 'ECG-gated' as the frame rate on a protocol allows the user to specify the location and length of projection acquisition within the cardiac cycle. Specifically, the Cardiac Phase Center (CPC) marks the delay time after the QRS complex is detected in percentage of the cardiac cycle (0-100) and the Cardiac Phase Width (CPW) defines the time duration in percentage of the cardiac cycle (0-100) either side of the CPC where the projection acquisition at the desired projection acquisition rate will occur. Under normal operating procedures, an example of a standard ECG-gated frame rate acquisition for a patient with a heart rate of 60 bpm with CPC = 70 and CPW = 10 (i.e. an acquisition window spanning 60-80% of the cardiac cycle) with a projection acquisition frame rate inside the CPW of 15 projections/second would result in 3 projections being acquired every cardiac cycle. To allow the projection acquisition to occur as required by the ACROBEAT scans, we selected CPC = 0 and CPW = 0, corresponding to allowing a single pulse acquisition to occur when a digital trigger is received at the ECG gating port. Specifically, a digital trigger is sent from the microcontroller (Figure 5) running the ACROBEAT software monitoring the ECG signal at the required time (i.e. at 70% the cardiac cycle), enabling the projections to be acquired as required.

Finally, to ensure a fair comparison between ACROBEAT and conventional acquisition, the conventional acquisition was also implemented using the TACS and a CORO ECG-gated protocol (90 kV, 24 mAs) on the ARTIS pheno. The conventional protocol implemented using the TACS acquires 248 projections at a constant rate over a 200° arc with constant velocity, resulting in a scan time of 8.3 s. Note this is almost double the scan time of the clinically available protocol simulated in Section 2B. As both the ACROBEAT and conventional scans have longer scan times compared to the simulation study, there will be an increase in the amount of artery motion observed. Further differences between the experimental implementation of the ACROBEAT and conventional scans are expanded in the discussion.

C.2 Physical Artery Phantom

A photograph of the simplistic physical artery phantom constructed for the proof-of-concept experimental study is provided in Figure 6 (A). Here, the expansion of the artery was accomplished by pumping water mixed with an iodine contrast agent through a silicon rubber tube, (Gecko Optical) with an inner diameter of 7 mm and outer diameter of 8 mm and was 50 mm in length, that was encased in Phytagel (Sigma Aldrich CAS 71010-52-1). More specifically, a single chamber test cell, orange outline in Figure 6, was constructed to encase the artery and tissue phantom. The inner cell, green outline in Figure 6, dimensions were 80 mm × 30 mm × 50 mm with a wall thickness of 5 mm. Two 3 mm diameter holes were drilled through both ends of the cell and barbs were fitted so that both the motor and reservoir connection tubes could be attached. A carotid artery and tissue phantom were created using silicon rubber tubing cast into Phytagel. The silicon rubber tubing was affixed to barbs on either side of the test cell. The tissue phantom was created by mixing 100 mL of distilled water and 2 g of Phytagel into a 500 mL beaker. The phantom mixture was heated and mixed to 90 °C and subsequently cooled to 80 °C before it was transferred into the test cell. The gel was allowed to cool to room temperature overnight and then the top plate of the test cell was fitted.

The carotid artery control system comprised of a laptop (MacBook Pro 2015, Apple, CA, USA), main controller board (Arduino Mega) and a motor control daughter board (Arduino Uno). The laptop interfaced to the main controller board via UART at 115200 baud enabling the communication of both an ECG and motion profile signal. On the main control board, the ECG signal was generated by converting it to a 12-bit analogue signal and outputting it on a cable. The main control board also forwarded the motion waveform to the daughter board via UART at 115200 baud which was subsequently converted to a PWM signal which controlled a 12 V NUZAMAS, NEW 12V High Pressure Diaphragm Self Priming Water Pump (Model-BR-3800). Using 2D fluoroscopic images acquired from a static position directly above the phantom with a frame rate of 10 fps, the physical artery phantom experiences a diameter expansion of 0.7 mm over the course of the cardiac cycle. The silicon tube is under pressure from both the water/iodine mixture being pumped through the tube and surrounding Phytagel, resulting in an elliptical expansion rather than circularity expansion of the tube. As such, up to 2 mm of diameter expansion over the cardiac cycle is experienced in some planes. An iodine contrast agent was used as a blood surrogate and pumped through the carotid artery and tissue phantom and discharged into a catchment reservoir.

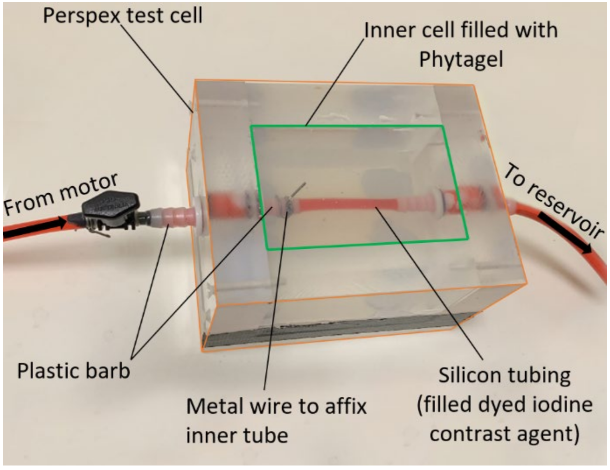

Figure 6. Physical artery and tissue phantom. Orange highlighted region indicates the test cell and the green highlighted region shows the inner cell housing the silicon tube embedded in Phytagel.

D. Artery Width Measurement

The data from each acquisition\trace pair acq, bpm were reconstructed using the Feldkamp-Davis-Kress (FDK) [28] algorithm implemented in the Reconstruction ToolKit (RTK) [27]. We used a Hann filter with frequency cut off of 0.9 and sinogram padding of 4 pixels to produce the 10 $X_{acq,bpm}$ volumes.

Artery width was estimated semi-automatically to reduce bias in the results. The N voxel values $x_{uw,acq,bpm}$ corresponding to a $w \times h \times l$ mm Region-of-Interest (ROI) subvolume of $X_{acq,bpm}$ were automatically windowed as $x_{acq,bpm} = \hat{a}x_{uw,acq,bpm} + \hat{b}$ where $(\hat{a}, \hat{b}) = \min_{a,b}\left\{\left\|x_{GT} - (ax_{uw,acq,bpm} + b)\right\|_2^2\right\}$ and x_{GT} is a vector of ground truth voxel values in the ROI. The $n_{acq,bpm}$ voxels corresponding to carotid were found by histogram segmentation, giving the carotid volume as $V_{acq,bpm} = n_{acq,bpm}$ mm^3.

In the simulation study, the carotid was modelled as two cylinders in the ROI each with length l and volume $\frac{1}{2}n_{acq,bpm}\text{mm}^3$. The carotid width was estimated as $w_{acq,bpm} = \sqrt{\frac{2n_{acq,bpm}}{\pi l}}$ mm. In the phantom study, the carotid was modelled as a single cylinder in the ROI with length l and volume $n_{acq}\,\mathrm{mm}^3$, giving a width estimate of $w_{acq} = \sqrt{\frac{4n_{acq}}{\pi l}}$ mm.

E. Image Quality Metrics

As the ground truth was available for the simulation studies, the image quality metrics of Root Mean Square Error (RMSE) and Structural Similarity Index (SSIM) were also utilized to assess image quality. RMSE was calculated as $RMSE(x_{acq,bpm}) = \frac{1}{\sqrt{N}}\left\|x_{acq,bpm} - x_{GT}\right\|_2$. Additionally, SSIM was computed as $SSIM = \frac{(2\mu_{GT}\mu_{acq,bpm}+c_1)(2\sigma_{acq,bpm,GT}+c_2)}{(\mu_{GT}^2+\mu_{acq,bpm}^2+c_2)(\sigma_{GT}^2+\sigma_{acq,bpm}^2+c_2)}$ [29] where μ and σ^2 denote voxel value means and variances, $c_1 = (0.01L)^2$ and $c_2 = (0.03L)^2$ where $L = (2^{\text{bits per voxel}} - 1)$ is the dynamic range of the volumes (number of possible voxel values).

III. Results

A. Simulation Study

For the $\overline{56}$, $\overline{64}$, $\overline{76}$, $\overline{86}$ and $\overline{100}$ bpm traces, the ACROBEAT scans took 35.6 s, 29.6 s, 22.6 s, 21.6 s and 31.7 s and acquired 88, 93, 90, 87 and 103 projections respectively. As highlighted in the methods section, the total scan time for an ACROBEAT scan is dependent on multiple factors including the patient's heart rate, scan parameters (e.g. length of the acquisition window and angular separation between projections) and mechanical constraints of the system. For the first 4 traces ($\overline{56}$, $\overline{64}$, $\overline{76}$, $\overline{86}$ bpm) the combination of heart rate, length of the acquisition window, required angular separation of the projections and mechanical constraints of the system, allows 3 projections to be acquired in each cardiac cycle. This allows an almost linear decrease in scan time with increasing heart rate. However, for the $\overline{100}$ bpm trace, only 2 projections can be acquired in each cardiac cycle. This results in a higher scan time than the other heart rates despite the higher heart rate. Comparing the total number of projections acquired using the two acquisition protocol, ACROBEAT enables an average reduction of 63%.

A sample of the reconstructed 3D images from simulating ACROBEAT and conventional acquisitions for the $\overline{56}$ bpm patient measured trace are shown in Figure 7 (A). The remaining 4 traces show the same visual trends, with an observable increased width in the carotid artery due to not accounting for the induced cardiac motion during imaging, Figure 7 (B)-(E).

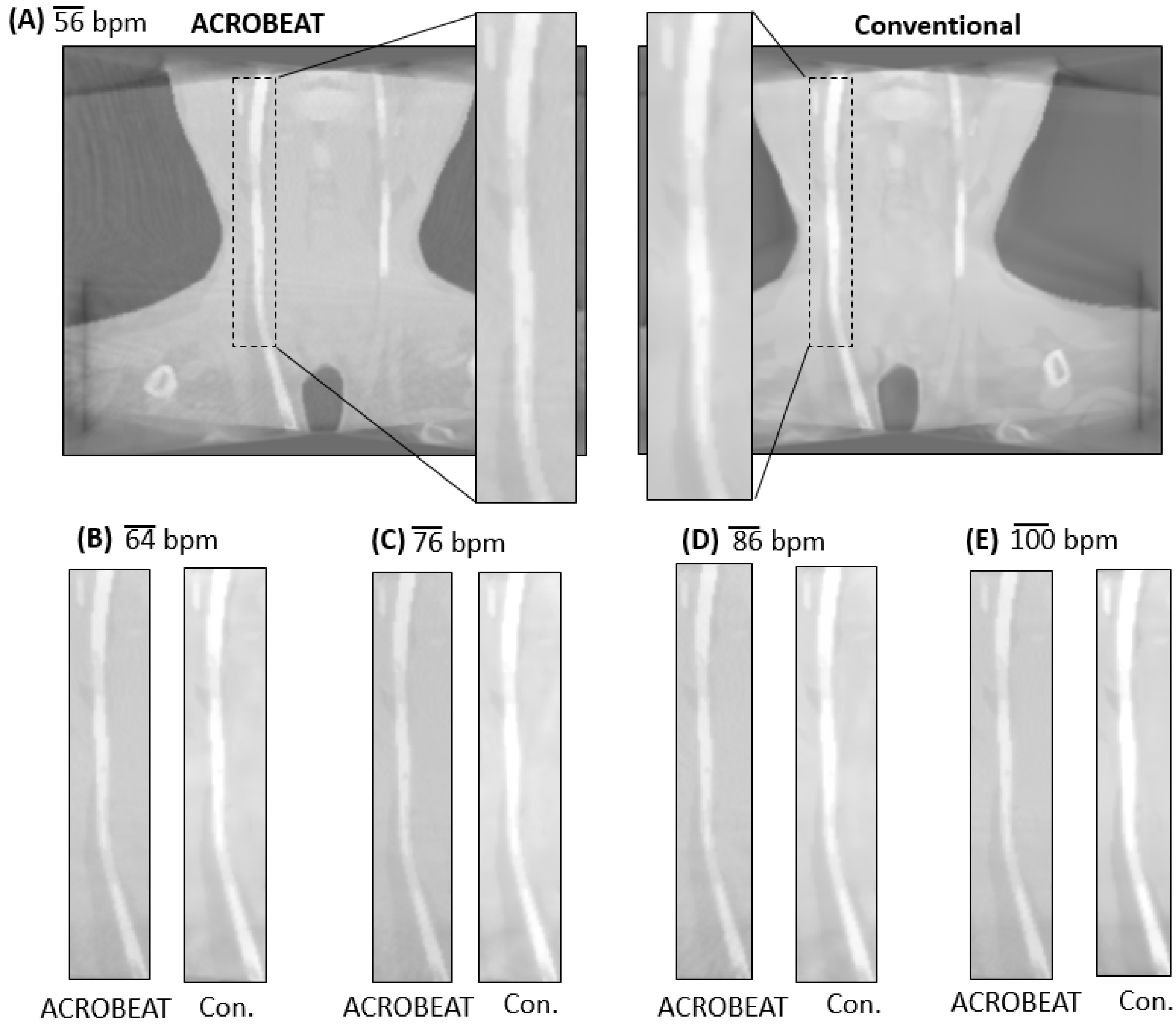

Figure 7. (A) Reconstructed 3D images (coronal view) showing the carotid arteries for ACROBEAT and conventional scans for the $\overline{56}$ bpm trace. The coronal view of only the left carotid artery from the reconstructed 3D images for the ACROBEAT and conventional scans of the $\overline{64}$, $\overline{76}$, $\overline{86}$ and $\overline{100}$ bpm traces are shown in (B) through (E) respectively.

The boxplots of the measured width of the carotid artery for all 5 traces from both the ACROBEAT and conventional acquisitions are provided in Figure 8 (A). There was no observable association between the average heart rate of the trace and the measured carotid width for ACROBEAT or the conventional acquisition. Across all 5 traces, ACROBEAT was able to lower the measured error in the carotid width, enabling a 65% reduction in carotid width measurement due to cardiac motion compared to a conventional acquisition, Figure 8 (B).

The boxplots of the RSME and SSIM for all 5 traces from both the ACROBEAT and conventional acquisition are provided in Figure 9. Compared to the conventional acquisition across all 5 traces, ACROBEAT enables a reduction in the RMSE by 11% and improves the SSIM by 27%.

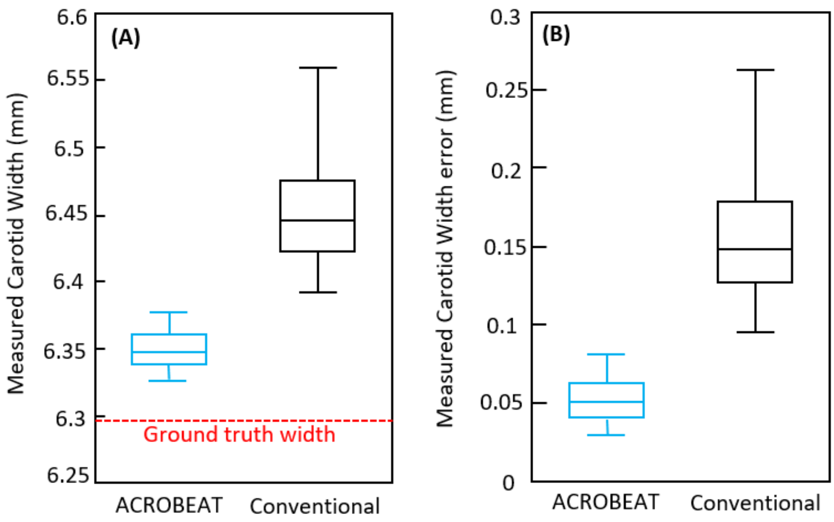

Figure 8. Boxplots of (A) the measured carotid artery width and (B) the measured carotid artery width error (defined as the absolute difference between the estimated ground truth and the measured carotid artery width) for all 5 traces using ACROBEAT (blue) and conventional (black) acquisition. For each box, the central line indicates the median, with the top and bottom edges indicating the 75th and 25th percentiles. The whiskers identify the maximum and minimum values of the data set.

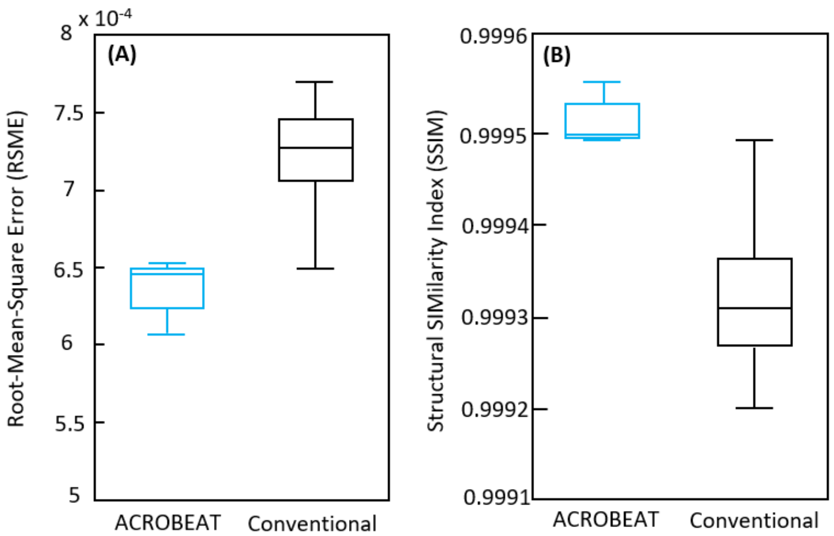

Figure 9. Boxplots of (A) the Root-Mean-Square-Error (RMSE) and (B) the Structural SIMilarity Index (SSIM) for all 5 traces using ACROBEAT (blue) and conventional (black) acquisition. For each box, the central line indicates the median, with the top and bottom edges indicating the 75th and 25th percentiles. The whiskers identify the maximum and minimum values of the data set.

B. Proof-of-concept Physical Phantom Experimental Study

Reconstructed 3D images from both imaging protocols are shown in Figure 10. The ACROBEAT scan acquired 100 projections, resulting in a 60% reduction in the total number of projections acquired compared to a conventional constant gantry velocity and projection pulse rate scan. Additionally, a noticeable difference in artery diameter can be observed between the two scans, with the ACROBEAT scan visually showing a narrower artery. The artery width quantification process calculated the diameter to be 10.4 mm with the single rotation constant gantry velocity and projection pulse rate and 8.75 mm using with ACROBEAT, compared with the static value of 8 mm.

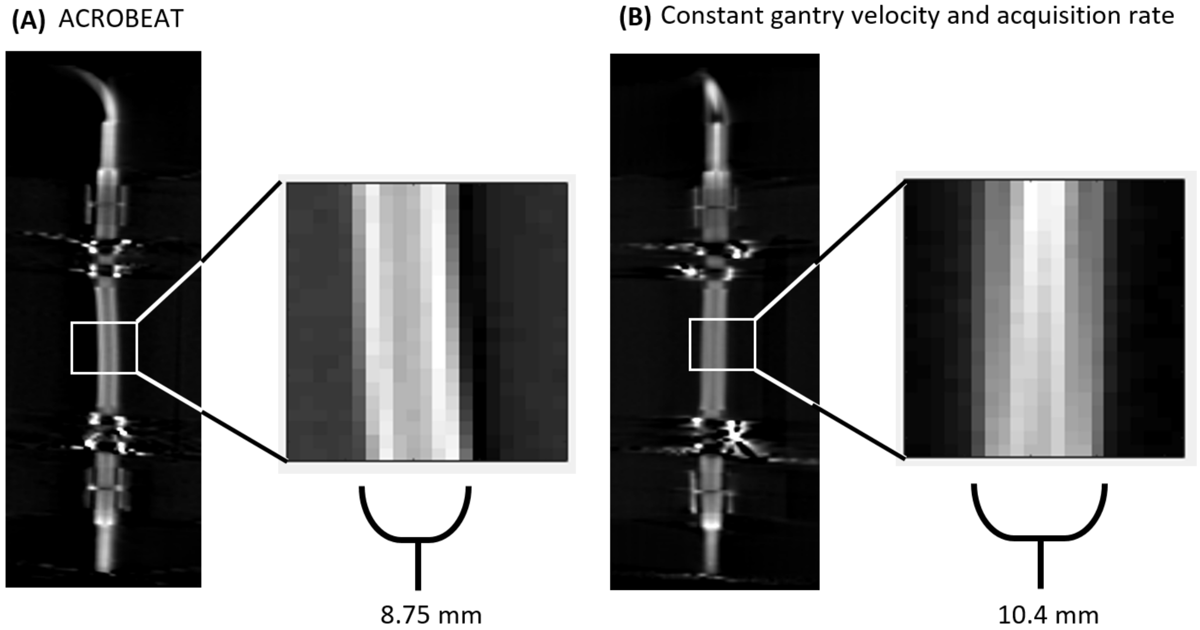

Figure 10. The reconstructed 3D images from (A) ACROBEAT and (B) a constant gantry velocity and projection acquisition rate scan. The known diameter of the artery in the phantom is 8 mm. Intensity window display [0.15, 0.08] mm^{-1}.

The total scan times increase from 8.3 s with the conventional single rotation constant gantry velocity and projection acquisition rate, to 103.2 s using ACROBEAT. The increase observed for both scans is due to the gantry velocity limits imposed when operating the ARTIS pheno with the TACS. However, the simulation studies are indicative of the scan times achievable with a dedicated imaging system.

IV. Discussion

The focus of this paper was imaging the carotid artery in the presence of cardiac pulsing in a simulation study and a proof-of-concept physical phantom experimental study using the dynamic imaging protocol ACROBEAT. In the simulation study, ACROBEAT was able to demonstrate its potential to reduce the total number of projections acquired while improving image quality compared to a conventional acquisition. Notably, it provides an average 63% reduction in the total number of projections acquired, across all patient measured traces considered. Further, ACROBEAT reduced the carotid artery width estimation error by 65%, reduced the RSME by 11% and improved the SSIM by 27% compared to a conventional acquisition.

In the proof-of-concept experimental study ACROBEAT was, for the first time, implemented on a clinical imaging system for applications in 3D artery imaging. ACROBEAT was again able to demonstrate its potential to reduce the total number of projections acquired and improve image quality compared to a conventional constant gantry velocity and projection pulse rate acquisition. Specifically, ACROBEAT enabled a 60% decrease in the total number projections acquired and a 21% decrease in the measured artery diameter compared to constant gantry velocity and acquisition rate acquisition.

3D CBCT imaging continues to grow in popularity in the interventional suite, especially for neuro-interventional procedures. Therefore, being able to provide an imaging protocol that has the potential to reduce the total number of projections and improve image quality will have a positive impact on a range of neuro-interventional procedures that utilize currently available 3D imaging [9, 30-32].

It should be noted that the amount of diameter expansion experienced by the physical artery phantom in the proof-of-concept experimental study was almost double (30%) what is reported in the literature (16%) [15, 16]. Unfortunately, the fidelity of the water pump used to deliver the pulsing within the carotid artery phantom was insufficient to allow precise control of the maximum change in diameter observed. Therefore, this proof-of-concept represents the worst case scenario with over 2 mm of diameter expansion within the carotid artery.

Further, for the experimental test case we ideally would have completed a direct comparison between ACROBEAT and the current commercially available DynaCT protocol on the Siemens ARTIS pheno. However, there is a significant amount of pre-processing that goes into both the individual 3D x-ray projections acquired and the final reconstructed volume that is not currently available to ACROBEAT projections and reconstructed volumes. This renders a direct comparison impossible. In future implementations, being able to access either the raw data or pre-processing would assist in improving the image quality of ACROBEAT scans and enable a direct comparison to clinically available protocols.

The current implementation of ACROBEAT on the Siemens ARTIS pheno via the TACS has notable limitations. Most noticeable is the joystick control that limits the maximum gantry velocity achievable, with 100% deflection corresponding to approximately 20 °/s. This is significantly lower than the maximum of 90 °/s for conventional acquisitions on the system. As a result, the scan times in the proof-of-concept experimental study are significantly longer than in the simulation study that used the mechanical constraints of the system operating normally. Specifically, the ACROBEAT scan time increased almost 3 times from 35.6 s to 103.2 s and the conventional scan time increased from 4 s to 8.3 s from the simulation study to proof-of-concept experimental implementation. Further, the gantry velocity limitations also prevented us from identifying the optimal injection rate and contrast density that ACROBEAT scans would utilize in the current implementation. The optimal injection rate and contrast density will be considered in future studies. Overall, it is hoped that in future implementations, having higher precision control over both the gantry position/velocity and x-ray projection acquisition would further assist in improving the image quality of the ACROBEAT scans.

As ACROBEAT progresses along the translational pipeline and the potential for the control algorithm to operate at the full capacity of the imaging system (i.e. matching the gantry velocity and acceleration under conventional operation), additional considerations such as gantry flex/vibration and image lag need to be taken into account. Not accounting correctly for gantry flex/vibration in the image reconstruction leads to artefacts that limit the image quality. To assist in mitigating these potential deleterious effects in our study, all the simulation studies took into account gantry acceleration/deceleration times to ensure a smooth gantry trajectory without sudden start/stops. To date the experimental implementations have been at low gantry velocities and accelerations, and as such these effects have not been noticeable. However, there is ongoing work in the literature addressing the gantry flex/vibration effects. These can be characterized as either image-based methods (such as registering current 2D projection data to a previously acquired 3D image [33, 34]) or marker-based methods (such as using fiducial markers [35] or using external cameras [36, 37]).

Currently, the focus of this work is imaging the carotid artery in the head and neck region. Within the head and neck region, there is negligible respiratory motion with the main source of motion arising from cardiac pulsing. However, if ACROBEAT is going to be used to imaging arteries and vessels in the thorax, both respiratory and cardiac motion would need to be taken into consideration. Additionally, it should be noted that any source of motion such as patient movement or swallowing, not just cardiac motion, will also negatively affect image quality. These other sources of motion would need to be dealt with using complementary motion management techniques, such as gating based on surface monitoring. Any additional motion management techniques may increase overall image acquisition time, which would need to be balanced with operational expediency.

In future implementations, performance could be further enhanced by coupling the unique image acquisition proposed by ACROBEAT with projection sharing techniques [38] and motion compensated reconstruction techniques [39].

V. Conclusion

This study is the first application of a novel adaptive imaging protocol, ACROBEAT, outside of the thoracic region. It shows that ACROBEAT has the potential to provide sharper and safer images for intracranial interventional procedures negatively affected by cardiac motion.

Acknowledgements

This was supported in part by a Research Agreement and Funding from Siemens Healthcare GmbH, Erlangen, Germany, Cancer Australia Priority Driven Collaborative Project Grant 1123068 and an

Australian NHMRC Senior Principal Research Fellowship. The authors gratefully acknowledge the input of Chiheb Dahmani, PhD in the Advanced Therapies Business Area of Siemens Healthineers for identifying that carotid artery distortion is an issue and providing details of the magnitude of the problem for different interventional procedures. The authors also acknowledge Dr A. Heitor Reis from the School of Science and Technology, University of Evora for personal communications. The authors acknowledge the facilities and scientific and technical assistance of Sydney Imaging, a Core Research Facility at the Charles Perkins Centre, University of Sydney. The authors would also like to acknowledge Siemens Australia Engineer Kevin Stephens for his technical support in the operation of the ARTIS pheno and TACS as well as ACRF Image X Institute Design and Communication Officer Julia Johnson for graphical support and Research Assistant Siqi Chen for her preliminary work on the phantom design.

Disclaimer: The concept and information presented in this paper are based on research and is not commercially available. Due to regulatory reasons its future availability cannot be guaranteed.

References

[1] J.L. Brisman, J.K. Song, and D.W. Newell,"Cerebral Aneurysms," *The New England Journal of Medicine*. 355 (9): p. 928-939, 2006.

[2] E.S. Connolly, Jr. and R.A. Solomon,"Management of Symptomatic and Asymptomatic Unruptured Aneurysms," *Neurosurgery Clinics*. 9 (3): p. 509-524, 1998.

[3] E.F.M. Wijdicks, D.F. Kallmes, E.M. Manno, J.R. Fulgham, and D.G. Piepgras,"Subarachnoid Hemorrhage: Neurointensive Care and Aneurysm Repair," *Mayo Clinic Proceedings*. 80 (4): p. 550-559, 2005.

[4] J.B. Bederson, I.A. Awad, D.O. Wiebers, D. Piepgras, E.C. Haley, Jr., T. Brott, G. Hademenos, D. Chyatte, R. Rosenwasser, and C. Caroselli,"Recommendations for the management of patients with unruptured intracranial aneurysms: A statement for healthcare professionals from the Stroke Council of the American Heart Association," *Circulation*. 102 (18): p. 2300-8, 2000.

[5] S.C. Johnston, S. Selvin, and D.R. Gress,"The burden, trends, and demographics of mortality from subarachnoid hemorrhage," *Neurology*. 50 (5): p. 1413-1418, 1998.

[6] P.A. Gardner, F. Vaz-Guimaraes, B. Jankowitz, M. Koutourousiou, J.C. Fernandez-Miranda, E.W. Wang, and C.H. Snyderman,"Endoscopic Endonasal Clipping of Intracranial Aneurysms: Surgical Technique and Results," *World Neurosurgery*. 84 (5): p. 1380-1393, 2015.

[7] A. Molyneux and R. Kerr,"International Subarachnoid Aneurysm Trial (ISAT) of neurosurgical clipping versus endovascular coiling in 2143 patients with ruptured intracranial aneurysms: A randomized trial," *Journal of Stroke and Cerebrovascular Diseases*. 11 (6): p. 304-314, 2002.

[8] P.I. D'Urso, G. Lanzino, H.J. Cloft, and D.F. Kallmes,"Flow Diversion for Intracranial Aneurysms," *Stroke*. 42 (8): p. 2363-2368, 2011.

[9] G. Benndorf, C.M. Strother, B. Claus, R. Naeini, H. Morsi, R. Klucznik, and M.E. Mawad,"Angiographic CT in Cerebrovascular Stenting," *American Journal of Neuroradiology*. 26 (7): p. 1813-1818, 2005.

[10] R. Anxionnat, S. Bracard, X. Ducrocq, Y. Trousset, L. Launay, E. Kerrien, M. Braun, R. Vaillant, F. Scomazzoni, A. Lebedinsky, and L. Picard,"Intracranial aneurysms: clinical value of 3D digital subtraction angiography in the therapeutic decision and endovascular treatment," *Radiology*. 218 (3): p. 799, 2001.

[11] D. Ding, R.M. Starke, C.R. Durst, J.R. Gaughen, A.J. Evans, M.E. Jensen, and K.C. Liu,"DynaCT imaging for intraprocedural evaluation of flow-diverting stent apposition during endovascular

treatment of intracranial aneurysms," *Journal of Clinical Neuroscience*. 21 (11): p. 1981-1983, 2014.

[12] G. Richter, T. Engelhorn, T. Struffert, M. Doelken, O. Ganslandt, J. Hornegger, W.A. Kalender, and A. Doerfler,"Flat panel detector angiographic CT for stent-assisted coil embolization of broad-based cerebral aneurysms," *AJNR. American journal of neuroradiology*. 28 (10): p. 1902-8, 2007.

[13] N.S. Heran, J.K. Song, K. Namba, W. Smith, Y. Niimi, and A. Berenstein,"The Utility of DynaCT in Neuroendovascular Procedures," *American Journal of Neuroradiology*. 27 (2): p. 330-332, 2006.

[14] P. Mordasini, F. Al-Senani, J. Gralla, D.-D. Do, C. Brekenfeld, and G. Schroth,"The use of flat panel angioCT (DynaCT) for navigation through a deformed and fractured carotid stent," *Neuroradiology*. 52 (7): p. 629-632, 2010.

[15] R.E. Latchaw and S.L. Albers,"Imaging the cervical vasculature," *Progress in cardiovascular diseases*. 59 (6): p. 555-584, 2017.

[16] K. Perktold and G. Rappitsch,"Computer simulation of local blood flow and vessel mechanics in a compliant carotid artery bifurcation model," *Journal of Biomechanics*. 28 (7): p. 845-856, 1995.

[17] T. Reynolds, C.-C. Shieh, P.J. Keall, and R.T. O'Brien,"Towards patient connected imaging with ACROBEAT: Adaptive CaRdiac cOne BEAm computed Tomography," *Physics in Medicine & Biology*. 64 (6): p. 065006, 2019.

[18] T. Reynolds, C.-C. Shieh, P.J. Keall, and R.T. O'Brien,"Dual cardiac and respiratory gated thoracic imaging via adaptive gantry velocity and projection rate modulation on a linear accelerator: A Proof-of-Concept Simulation Study," *Medical Physics*. 46 (9): p. 4116-4126, 2019.

[19] S. Mao, M.J. Budoff, L. Bin, and S.C.K. Liu,"Optimal ECG Trigger Point in Electron-Beam CT Studies: Three Methods for Minimizing Motion Artifacts," *Academic Radiology*. 8 (11): p. 1107-1115, 2001.

[20] A.C. Weustink, N.R. Mollet, F. Pugliese, W.B. Meijboom, K. Nieman, M.H. Heijenbrok-Kal, T.G. Flohr, L.A.E. Neefjes, F. Cademartiri, P.J.d. Feyter, and G.P. Krestin,"Optimal Electrocardiographic Pulsing Windows and Heart Rate: Effect on Image Quality and Radiation Exposure at Dual-Source Coronary CT Angiography," *Radiology*. 248 (3): p. 792-798, 2008.

[21] H. Isma'eel, Y.S. Hamirani, R. Mehrinfar, S. Mao, N. Ahmadi, V. Larijani, S. Nair, and M.J. Budoff,"Optimal phase for coronary interpretations and correlation of ejection fraction using late-diastole and end-diastole imaging in cardiac computed tomography angiography: implications for prospective triggering," *Int J Cardiovasc Imaging*. 25 (7): p. 739-749, 2009.

[22] P.W. Segars, G. Sturgeon, S. Mendonca, J. Grimes, and B.M.W. Tsui,"4D XCAT phantom for multimodality imaging research," *Medical Physics*. 37 (9): p. 4902-4915, 2010.

[23] J.S. Au, H. Yli-Ollila, and M.J. MacDonald,"An assessment of intra-individual variability in carotid artery longitudinal wall motion: recommendations for data acquisition," *Physiological Measurement*. 39 (9): p. 09NT01, 2018.

[24] J. Tat, J.S. Au, P.J. Keir, and M.J. MacDonald,"Reduced common carotid artery longitudinal wall motion and intramural shear strain in individuals with elevated cardiovascular disease risk using speckle tracking," *Clinical Physiology and Functional Imaging*. 37 (2): p. 106-116, 2017.

[25] M.A. García-González, A. Argelagós, M. Fernández-Chimeno, and J. Ramos-Castro. "Differences in QRS Locations due to ECG Lead: Relationship with Breathing". Cham, 2014, pp. 962-964

[26] M.A. García-González, A. Argelagós-Palau, M. Fernández-Chimeno, and J. Ramos-Castro. "A comparison of heartbeat detectors for the seismocardiogram". in *Computing in Cardiology 2013*. 2013, pp. 461-464

[27] S. Rit, M.V. Oliva, S. Brousmiche, R. Labarbe, D. Sarrut, and G.C. Sharp,"The Reconstruction Toolkit (RTK), an open-source cone-beam CT reconstruction toolkit based on the Insight Toolkit (ITK)," *Journal of Physics: Conference Series*. 489 (1): p. 012079, 2014.

[28] L.A. Feldkamp, L.C. Davis, and J.W. Kress,"Practical cone-beam algorithm," *J. Opt. Soc. Am. A*. 1 (6): p. 612-619, 1984.

[29] W. Zhou, A.C. Bovik, H.R. Sheikh, and E.P. Simoncelli,"Image quality assessment: from error visibility to structural similarity," *IEEE Transactions on Image Processing*. 13 (4): p. 600-612, 2004.

[30] T.F. Flood, I.M.J. van der Bom, L. Strittmatter, A.S. Puri, G.M. Hendricks, A.K. Wakhloo, and M.J. Gounis,"Quantitative analysis of high-resolution, contrast-enhanced, cone-beam CT for the detection of intracranial in-stent hyperplasia," *Journal of NeuroInterventional Surgery*. 7 (2): p. 118-125, 2015.

[31] A. Hochmuth, U. Spetzger, and M. Schumacher,"Comparison of three-dimensional rotational angiography with digital subtraction angiography in the assessment of ruptured cerebral aneurysms," *AJNR. American journal of neuroradiology*. 23 (7): p. 1199-205, 2002.

[32] U. Missler, C. Hundt, M. Wiesmann, T. Mayer, and H. Brückmann,"Three-dimensional reconstructed rotational digital subtraction angiography in planning treatment of intracranial aneurysms," *European radiology*. 10 (4): p. 564-8, 2000.

[33] S. Ouadah, J.W. Stayman, G. Gang, A. Uneri, T. Ehtiati, and J.H. Siewerdsen,"Self-Calibration of Cone-Beam CT Geometry Using 3D-2D Image Registration: Development and Application to Task-Based Imaging with a Robotic C-Arm," *Proceedings of SPIE--the International Society for Optical Engineering*. 9415 p. 2015.

[34] W. Wein, A. Ladikos, and A. Baumgartner. "Self-calibration of geometric and radiometric parameters for cone-beam computed tomography". in *Fully three-dimensional image reconstruction in radiology and nuclear medicine Proceedings*. Germany, 2011, pp. 480

[35] C. Syben, B. Bier, M. Berger, A. Aichert, R. Fahrig, G. Gold, M. Levenston, and A. Maier. "JOINT calibration and motion estimation in weight-bearing cone-beam CT of the knee joint using fiducial markers". in *2017 IEEE 14th International Symposium on Biomedical Imaging (ISBI 2017)*. 2017, pp. 494-497

[36] F. Albiol, A. Corbi, and A. Albiol,"Geometrical Calibration of X-Ray Imaging With RGB Cameras for 3D Reconstruction," *IEEE transactions on medical imaging*. 35 (8): p. 1952-61, 2016.

[37] M. Mitschke and N. Navab,"Recovering the X-ray projection geometry for three-dimensional tomographic reconstruction with additional sensors: attached camera versus external navigation system," *Medical image analysis*. 7 (1): p. 65-78, 2003.

[38] R.T. O'Brien, J. Kipritidis, C.C. Shieh, and P.J. Keall,"Optimizing 4DCBCT projection allocation to respiratory bins," *Physics in medicine and biology*. 59 (19): p. 5631-49, 2014.

[39] S. Sauppe, A. Hahn, M. Brehm, P. Paysan, D. Seghers, and M. Kachelrieß, *Five-dimensional motion compensation for respiratory and cardiac motion with cone-beam CT of the thorax region*. SPIE Medical Imaging. Vol. 9783. 2016: SPIE.

[40] Dillon, O., O’Brien, R., Shieh, C., Keall. P. 2019. Evaluating Reconstruction Algorithms for Respiratory Motion Guided Acquisition. 2020. *Phys. Med. Biol.*

[41] C.-C. Shieh, Y. Gonzalez, B. Li, X. Jia, S. Rit, C. Mory, M. Riblett, G. Hugo, Y. Zhang, L. Ren and P. Keall, "SPARE: SPArse-view REconstruction challenge for 4D cone-beam CT from a one-minute scan," *Medical Physics,* vol. 46, no. 9, pp. 3799-3811, 2019.